VERTIV WHITE PAPER

Experimental lessons of an organic Rankine cycle applied for waste heat recovery in a data center environment

This white paper contains the salient points from a dissertation entitled Power Usage Effectiveness Improvement of High-Performance Computing by use of Organic Rankine Cycle Waste Heat Recovery by Russ Tipton

Authors:

Russell Tipton
Gregory Kremer
Muhammad Ali

Abstract

Organic Rankine cycle (ORC) is a preferred method to recover mechanical energy from low-quality waste heat. An ORC system replicating a 30kW liquid-cooled high performance compute rack of servers in data center application has been designed, fabricated, and tested to capture the server waste heat and convert a portion to electricity while transporting the heat to ambient air. The working fluid is compliant with contemporary environmental, health, and safety (EH&S) requirements and is a zeotropic blend to improve heat exchange effectiveness. The full load power usage effectiveness (PUE) is 1.02 compared to the 1.6 to 2.2 range in small data centers. [1] *Practical implications and limits for ORC system components are evaluated.*

Introduction

Similar work was done at a lab-scale[2]. In contrast this study:

- Utilized a low GWP non-toxic working fluid with improved EH&S acceptance.
- Accounted for the parasitic losses of thermal transport from heat source and to heat sink.
- Ensured ORC components had reliability acceptable for data center application.
- Discovered a minimum differential limit between heat source and heat sink to provide stable scroll expander operation.

Increasing demand for compute and a drive toward sustainability encourages efforts to recover and reuse waste heat from data centers. An ORC can be used to convert a portion of waste heat recovered from data centers on its path to outdoor ambient [3]. With low quality waste heat, it is important to minimize temperature losses along the thermal transport path. This study focuses on waste heat captured in liquid cooled servers at a leaving temperature of 58°C. A fully populated rack would produce up to 40kW waste heat [4]. Ashburn, VA, USA is a data center hub [5]. Ashburn'soutdoor temperature ranges from -14°C to 35°C with an average of 14°C[6]. Ashburn's climate is temperate, typical of population centers where data would be consumed, and in close proximity to large information consumers – Washington, DC, Baltimore, MD, and Philadelphia, PA. The built environment must comply with contemporary EH&S requirements. The challenge becomes evaluating the viability of an ORC waste heat recovery (WHR) system to cool high performance compute (HPC) equipment given EH&S requirements, the operating window of HPC equipment, and environmental conditions at the data center site.

Materials and Methods

The design point for a modular ORC WHR system becomes **~40kW, T_H=58°C,** and **T_L=14°C**. The heat sink temperature range is **-14°C≤T_L≤35°C**. Specific EH&S requirements are ozone depletion potential **(ODP) = 0**[7], global warming potential **(GWP) <650**, and ASHRAE safety rating A1 or A2L – nontoxic, and non- or mildly-flammable [8].

Problem definition

A temperature-entropy diagram of an ORC is shown in Fig. 1. An ideal ORC consists of

(a) isentropic compression of liquid, states 1 to 2s;

(b) isobaric heating to saturated liquid followed by isobaric, isothermal evaporation, states 2s to 3;

(c) isentropic expansion of vapor, states 3 to 4s; and

(d) isobaric de-superheat followed by isobaric, isothermal condensation, states 4s to 1.

Because real equipment and processes must be used, points 2 and 4 result from non-isentropic compression and expansion, respectively. A high-level schematic of an ORC system is shown in Fig. 2. Thermal transport and thermodynamic relationships can be derived from these figures.

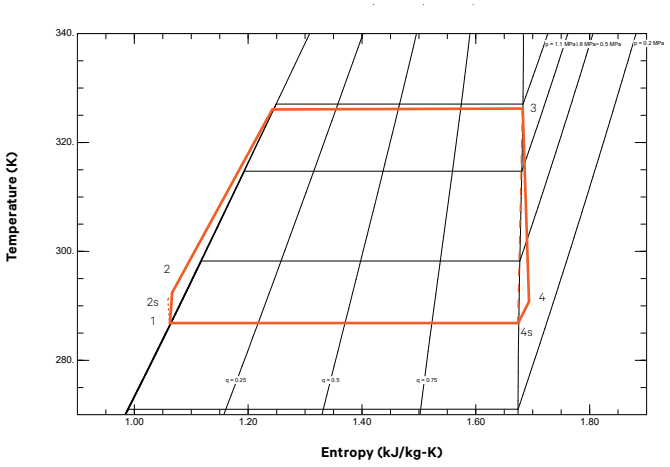

Figure 1. *Temperature entropy diagram of an organic Rankine cycle*

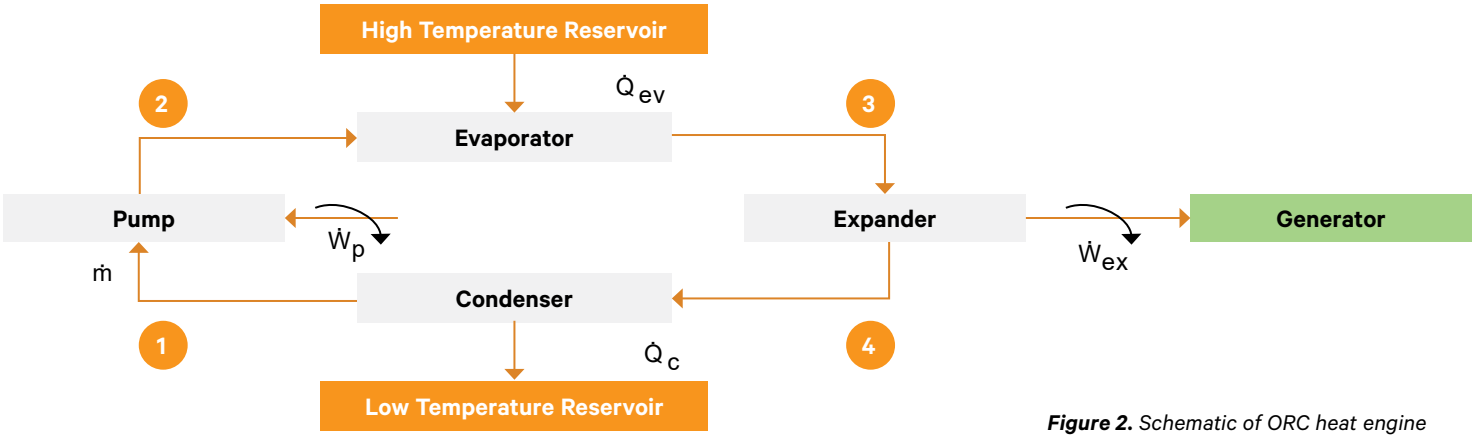

Figure 2. *Schematic of ORC heat engine*

For constant flow of the ORC working fluid, the first law of thermodynamics, as a macroscopic energy balance, states[9]:

$$\dot{Q}-\dot{W}=\dot{m}(\Delta h+\Delta k_P+\Delta k_E) \quad (1)$$

Work consumed by the pump:

$$\dot{W}_p=\dot{m}(h_2-h_1)=\dot{m}(h_{2s}-h_1)/\eta_p \quad (2)$$

Waste heat addition to the working fluid at the evaporator:

$$\dot{Q}_{ev}=\dot{m}(h_3-h_2) \quad (3)$$

Work generated by the expander:

$$\dot{W}_{ex}=\dot{m}(h_3-h_4)=\dot{m}(h_3-h_{4s})\eta_{ex} \quad (4)$$

Heat rejected from the condenser:

$$\dot{Q}_c=\dot{m}(h_4-h_1) \quad (5)$$

Exergy destruction rate equations are[10]:

$$\dot{I}_p=T_0\dot{m}(s_2-s_1) \quad (6)$$

$$\dot{I}_{ev}=T_0\dot{m}[(s_3-s_2)-(h_3-h_2)/T_H] \quad (7)$$

$$\dot{I}_{ex}=T_0\dot{m}(s_4-s_3) \quad (8)$$

$$\dot{I}_c=T_0\dot{m}[(s_1-s_4)-(h_1-h_4)/T_L] \quad (9)$$

$$\dot{I}_{tot}=\dot{I}_p+\dot{I}_{ev}+\dot{I}_{ex}+\dot{I}_c=$$
$$=T_0\dot{m}[-(h_3-h_2)/T_H-(h_1-h_4)/T_L] \quad (10)$$

Major ORC components to be selected for the test apparatus are:

- Working fluid
- Heat source
- Evaporator
- Expander
- Condenser
- Liquid pump
- Heat sink

Working fluid

The working fluid is selected for optimum thermodynamic and transport properties while complying with contemporary EH&S requirements. Table 1 enumerates working fluid properties for optimum ORC performance [11-13]. A prime set of candidates, shown in Table 2, was established by screening those of the heating, ventilation, air conditioning, and refrigeration (HVACR) industry in their attempt to comply with EH&S requirements. The heat source is a stream of warm water and the heat sink is a stream of ambient air both of which will experience temperature change during heat flow. Zeotropic mixtures exhibit temperature change in the phase change process between liquid and vapor. Thus, the phase change temperature glide of zeotropic mixtures was considered to reduce the heat quality loss of evaporation and condensing processes. REFPROP version 10 [14] is used to determine thermodynamic properties for this analysis. The resulting ORC working fluid is a zeotropic blend of R1233zd(E) and R1234ze(E) 20% to 80% by mass. Its properties include a predicted 50% of Carnot efficiency, highest net power output, ODP=0, GWP=5, and ASHRAE A2L.

Thermodynamic	ICT ORC
Low liquid specific heat	Yes
High latent heat	Yes
Isentropic or dry fluids	Yes
Low specific volumes	Yes
Moderate pressures in the heat exchangers	Yes
Freezing point below the lowest operating temperature in the cycle	Yes
Normal boiling point below the lowest operating temperature in the cycle	Yes

Functional	ICT ORC
Chemical stability at the maximum operating temperature in the cycle	Yes
Noncorrosive and compatible with system materials and lubricating oil	Yes
Low ozone depletion potential (ODP)	0
Low global warming potential (GWP)	<500
Short atmospheric lifetime (ALT)	Yes
Low toxicity	ASHRAE A
Low, if not zero, flammability	ASHRAE 1 or 2L

Table 1. *Working fluid properties corresponding to the ICT ORC application*

Working fluid	REFPROP name
R1234yf	R1234yf
R1234ze(E)	R1234ze(E)
R1233zd(E)	R1233zd(E)
R450A Molar	R134a/R1234ze; 0.447/0.553
R513A Molar	R1234yf/R134a; 0.533/0.467

Table 2. *Working fluid candidates to thermodynamically analyze and their REFPROP name*

Heat Source

For the heat source, an array of immersion electric heaters, water pump, filter, and expansion tank are selected with total power output of 45kW using 480-3-60 electrical source. A variac is used to control the waste heat output.

Expander

For a design point of 40kW with 58C TH, 14C TL, and the R1233zd(E) / R1234ze(E) 20% / 80% by mass working fluid, the required mass flow rate is 0.203 kg/s, with pressure ratio, inlet to outlet, 2.27. The resulting volume ratio, inlet to outlet, and inlet volume flow rate are 2.36 and 0.00474 m3/s, respectively. A 5K temperature difference between TL and condensing temperature and TH and the evaporating temperature is used. An Air Squared E22H038B-L-SH semi-hermetic scroll expander has up to 85% volumetric efficiency, volume ratio of 3.25, 73 cm3/rev displacement, and 2,600 rpm maximum speed [15] which provides inlet volume flow rate of 0.00316 m3/s. Scroll expanders are not available in a wide range of capacities. The displacement of the selected Air Squared expander is predicted to transport a waste heat flow of ~30kW.

Evaporator

A brazed plate heat exchanger is commonly used for water to refrigerant evaporator applications. Utilizing sizing routine from ASHRAE Fundamentals Handbook [16] a SWEP B250ASHx80/1P was selected.

Condenser

Although micro-channel finned surface heat exchangers are preferred for condensing, circuiting flexibility for the test apparatus was best achieved by using a traditional finned tube heat exchanger. EVAP-COND [17] and Bohn Coil Performance charts [18] were used to size and circuit an eight row 1.07 m long x 1.32 m wide coil with 3/8" (9.52 mm) diameter tubes on 1" (25.4 mm) staggered spacing and 0.006" (0.15 mm) thick corrugated fins. A Zeihl-Abegg FN080-ZIK.GL.V7P3 electronically commutated (EC) motor with aerodynamically efficient propeller fan was used [19] to supply ~0.33 m3/s airflow.

Liquid pump

The performance required of the liquid pump for 30kW heat load is 0.152 kg/s at 0.460 MPa head. An MTH HP31 is a regenerative turbine pump that has this pressure / flow capability and is designed to pump volatile liquids [20]. The ORC operates with liquid entering the pump near saturation and requires operation without experiencing cavitation. An evaluation of the HP31 was made to determine the net positive suction head required by the HP31 with the selected working fluid. The HP31 performance with the selected working fluid was also evaluated. Table 3 and Figure 3 show the results of this evaluation. The 2.1 m liquid column and 3K subcooling become a test apparatus design constraint where the condenser liquid outlet must be ≥2.1 m above the pump inlet and the condenser is sized to provide 3K subcooling.

Pump speed	Working fluid	Mass flow rate	NPSHr	NPSHa	NPSHa *liquid column*	NPSHa *subcool*	Subcool
Hz		kg/s	m	m	M	m	K
60	R1234ze(E) / R1233zd(E) 80 / 20 mass	0.19	5.7	6.3	2.1	4.2	3.3
55		0.18	5.3	5.8	2.1	3.7	2.9
50		0.16	5.4	5.9	2.1	3.8	3

Table 3. *NPSHr and subcooling required*

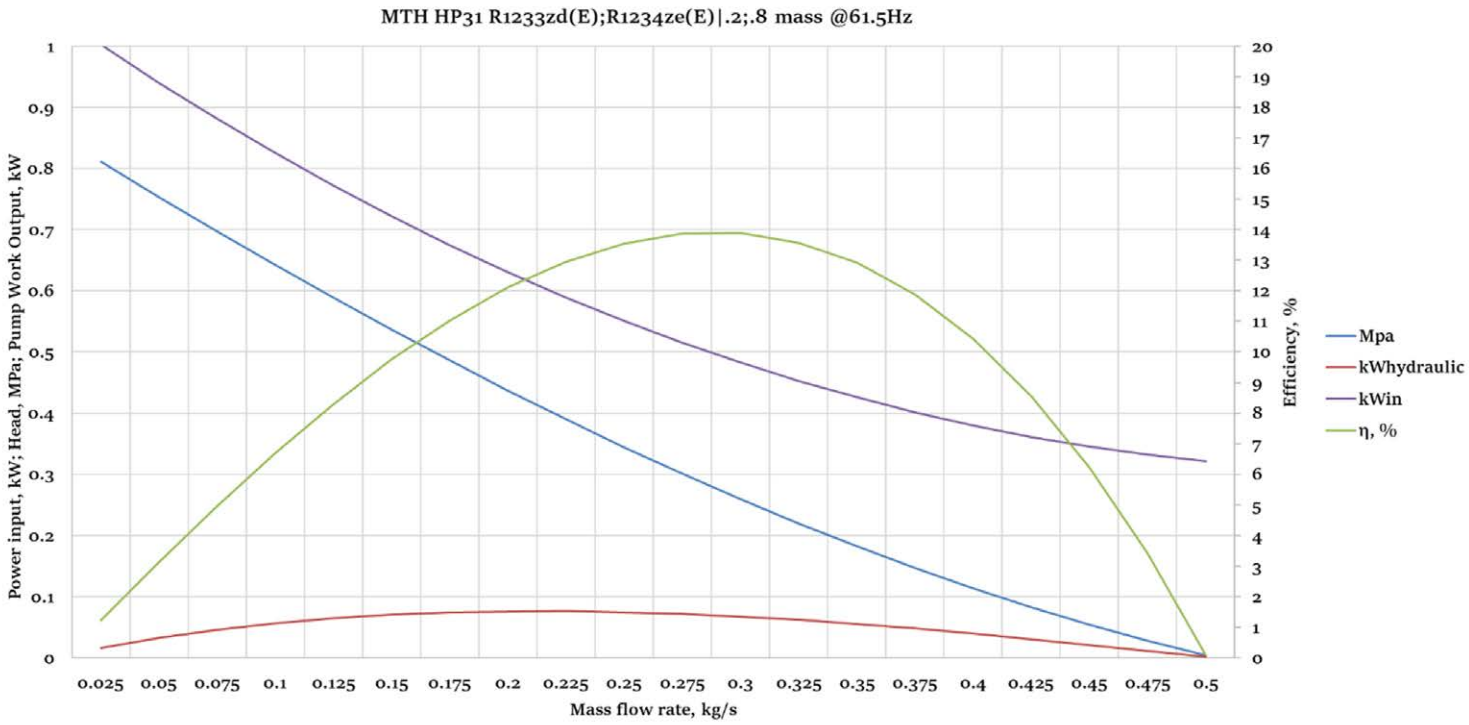

Figure 3. *MTH HP31 performance, R1233zd(E); R1234ze(E)|.2;.8 mass ~60Hz*

Heat sink

For the heat sink, the condenser and liquid pump will be enclosed in an environmental chamber that can provide constant temperature control while removing the ≤30kW heat of condensation plus the condenser fan motor heat.

Test apparatus and instrumentation

Figure 4 shows the configuration of the test apparatus. The liquid pump is the lowest part and the vertical distance to the condenser outlet is 2.1 m above the liquid pump inlet. A check valve prevents reverse flow during off-cycle. An accumulator prevents large amounts of liquid from entering the expander. Rather the liquid oil and any unevaporated working fluid are fed through as a mist that will not damage the scroll set. The evaporator was determined to require 25% of its area to remove the subcooling from the entering liquid stream. Thus, the evaporator is positioned with the condenser liquid outlet and evaporator bottom 25% line in horizontal alignment. To eliminate off-cycle liquid migration to a cold spot, low Watt density heat is added to the accumulator, expander housing, and vapor riser to the condenser inlet.

Figure 5 shows a piping and instrumentation diagram (P&ID). PT are laboratory grade 4-20 mA pressure transducers. TE are 100Ω platinum RTDs. PT and TE are placed at each state point in the ORC. TC are type T thermocouples strapped to outside of tubing. VAW measures Voltage, Amperage, and Wattage for each electrical component. FWF is a Coriolis effect mass flow meter for the ORC working fluid. FWTR is an electromagnetic volume flow meter for the heat source water. TQ and RPM are the expander torque and speed. Table 4 is a listing of the measurements for the ORC test apparatus.

Each instrument is calibrated annually by an ISO 17025 General requirements for the competence of testing and calibration laboratories accredited test laboratory. PT, TE, and TC are calibrated by comparison to ISO 17025 calibrated pressure and temperature standards with accuracy ≥4X that desired for the measurements. Correction factors are automatically applied in the LabVIEW based test control system. Measurement accuracies are listed in Table 5. These will be applied in the uncertainty analysis to validate the testing results.

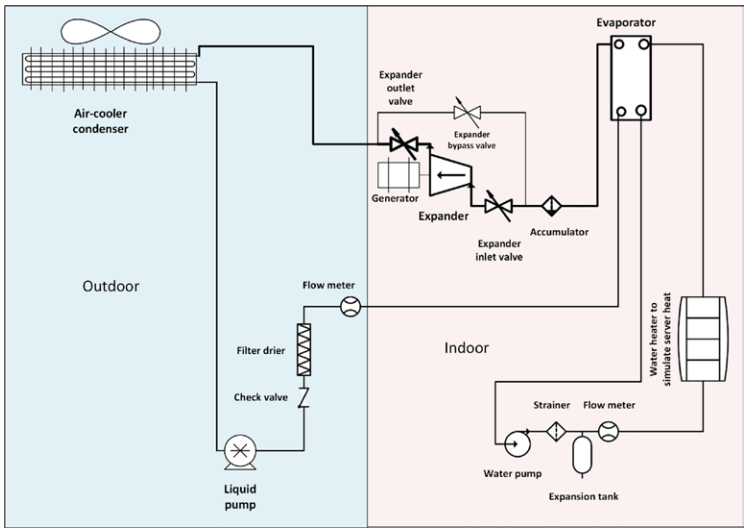

Figure 4. *Schematic of ORC ICT WHR apparatus*

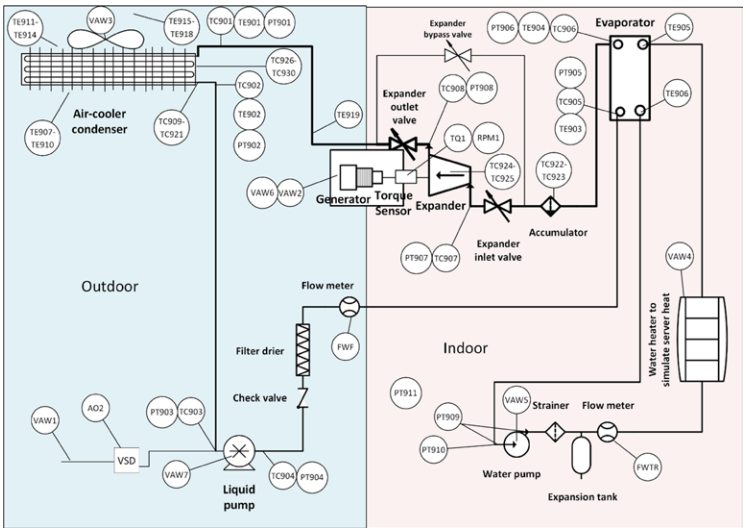

Figure 5. *P&ID of ORC test apparatus*

Label	Measurement	Label	Measurement	Label	Measurement
TC901	T4cnd-inTC (°F)	FWTR	H2O Flowrate (GPM)		HT SRC (Watts)
TC902	T1cnd-outTC (°F)	PT901	P4cnd -in (PSIG)		HT SRC (VAR)
TC903	T1liq-pmp-inTC (°F)	PT902	P1cnd -out (PSIG)		HT SRC (VA)
TC904	T2liq-pmp-outTC (°F)	PT903	P1liq-pmp-in (PSIG)		HT SRC Volts A
TC905	T2evap-inTC (°F)	PT904	P2liq-pmp-out (PSIG)		HT SRC Volts B
TC906	T3evap-outTC (°F)	PT905	P2evap-in (PSIG)	VAW4	HT SRC Volts C
TC907	T3exp-inTC (°F)	PT906	P3evap-out (PSIG)		HT SRC Amps A
TC908	T4exp-outTC (°F)	PT907	P3exp-in (PSIG)		HT SRC Amps B
TC909	TLiq-outcirc1 (°F)	PT908	P4exp -out (PSIG)		HT SRC Amps C
TC910	TLiq-outcirc2 (°F)	PT909	dPwater-pmp (PSID)		HT SRC Power Factor
TC911	TLiq-outcirc3 (°F)	PT910	Pwater-pmp-in (PSIG)		HT SRC Frequency (Hz)
TC912	TLiq-outcirc4 (°F)	PT911	Pbaro (inHg)		WTR PMP (Watts)
TC913	TLiq-outcirc5 (°F)	AO 2	Liquid Pump VFD (0-10V)		WTR PMP (VAR)
TC914	TLiq-outcirc6 (°F)		ORC Fluid Mass Flow (lb/min)		WTR PMP (VA)
TC915	TLiq-outcirc7 (°F)	FWF	ORC Fluid Temp (F)		WTR PMP Volts A
TC916	TLiq-outcirc8 (°F)		ORC Fluid Density (lb/ft3)		WTR PMP Volts B
TC917	TLiq-outcirc9 (°F)		LIQ PMP VFD (Watts)	VAW5	WTR PMP Volts C
TC918	TLiq-outcirc10 (°F)		LIQ PMP VFD (VAR)		WTR PMP Amps A
TC919	TLiq-outcirc11 (°F)		LIQ PMP VFD (VA)		WTR PMP Amps B
TC920	TLiq-outcirc12 (°F)		LIQ PMP VFD Volts A		WTR PMP Amps C
TC921	TLiq-outcirc13 (°F)		LIQ PMP VFD Volts B		WTR PMP Power Factor
TC922	Accum-L NoCal (°F)	VAW1	LIQ PMP VFD Volts C		WTR PMP Frequency (Hz)
TC923	Accum-R NoCal (°F)		LIQ PMP VFD Amps A		EXP GEN 2 (Watts)
TC924	EXP-HSG-L NoCal (°F)		LIQ PMP VFD Amps B		EXP GEN 2 (VAR)
TC925	EXP-HSG-R NoCal (°F)		LIQ PMP VFD Amps C		EXP GEN 2 (VA)
TC926	CND-RB R2-R3 NoCal (°F)		LIQ PMP VFD Power Factor		EXP GEN 2 Volts A
TC927	CND-RB R3-R4 NoCal (°F)		LIQ PMP VFD Frequency (Hz)		EXP GEN 2 Volts B
TC928	CND-RB R4-R5 NoCal (°F)		EXP GEN (Watts)	VAW6	EXP GEN 2 Volts C
TC929	CND-RB R5-R6 NoCal (°F)		EXP GEN (VAR)		EXP GEN 2 Amps A
TC930	CND-RB R6-R7 NoCal (°F)		EXP GEN (VA)		EXP GEN 2 Amps B
TE901	T4exp-cnd-RTD (°F)		EXP GEN Volts A		EXP GEN 2 Amps C
TE902	T1cnd-liq-pmp-RTD (°F)		EXP GEN Volts B		EXP GEN 2 Power Factor
TE903	T2Liq-pmp-evap-RTD (°F)	VAW2	EXP GEN Volts C		EXP GEN 2 Frequency (Hz)
TE904	T3evap-exp-RTD (°F)		EXP GEN Amps A		LIQ PMP (Watts)
TE905	Twater-inRTD (°F)		EXP GEN Amps B		LIQ PMP (VAR)
TE906	Twater-outRTD (°F)		EXP GEN Amps C		LIQ PMP (VA)
TE907	Tcnd-air-in-A (°F)		EXP GEN Power Factor		LIQ PMP Volts A
TE908	Tcnd-air-in-B (°F)		EXP GEN Frequency (Hz)		LIQ PMP Volts B
TE909	Tcnd-air-in-C (°F)		COND FAN (Watts)	VAW7	LIQ PMP Volts C
TE910	Tcnd-air-in-D (°F)		COND FAN (VAR)		LIQ PMP Amps A
TE911	Tcnd-air-out-A (°F)		COND FAN (VA)		LIQ PMP Amps B
TE912	Tcnd-air-out-B (°F)		COND FAN Volts A		LIQ PMP Amps C
TE913	Tcnd-air-out-C (°F)		COND FAN Volts B		LIQ PMP Power Factor
TE914	Tcnd-air-out-D (°F)	VAW3	COND FAN Volts C		LIQ PMP Frequency (Hz)
TE915	Tfan-out-A (°F)		COND FAN Amps A	TQ1	TQ513 excitation (VDC)
TE916	Tfan-out-B (°F)		COND FAN Amps B		TQ513 signal (mVDC)
TE917	Tfan-out-C (°F)		COND FAN Amps C	RPM1	Expander speed (RPM)
TE918	Tfan-out-D (°F)		COND FAN Power Factor		
TE919	Lqd Rsr (°F)		COND FAN Frequency (Hz)		

Table 4. *Measurements of ORC test apparatus*

Measurement	Instrument	Accuracy	Purpose	
Voltage (V)	Yokogawa WT230 / PR300	±0.25%	Liquid pump, VFD, water pump, condenser fan, heater (simulated server), permanent magnet generator	Energy balances
Current (A)		±0.25%		
Power (kW)		±0.3%		
Frequency (Hz)		±0.1%		Rotational Speed
Temperature (K)	Type T thermocouple	±0.15K	Attached to tubing	In/out temperature for each component
	100 Ω platinum RTD	±0.1K	ORC state points, water in / out Condenser air in / out	EOS input for thermodynamic properties, energy balance, TH, TL
Pressure (MPa)	Piezoresistive transducers	±1%	ORC state points	
Mass flow rate (kg/s)	MicroMotion Coriolis	±0.5%	ORC working fluid flow rate	Energy balance
Volume flow rate (lpm)	Siemens Mag-flow	±0.5%	Water flow rate	Energy balance

Table 5. *ORC system measurement instrument accuracy*

Results and Discussion

Test array

The array of tests run with ORC apparatus including operating conditions, waste heat input, expander output, liquid pump input, and net output are shown in Table 6. Conditions were TH ~58°C and ~63°C with TL ~14°C and ~8°C with load varying from 8kW to 30kW (roughly 25% increments). For the higher ambient, until input power was >75% the liquid pump power exceeded the expander output. For the lower ambient, the expander output exceeded the liquid pump input >50% load.

Test File	T_H (°C)	T_L (°C)	$\dot{Q}$ (kW)	$\dot{W}_{ex}$ (kW)	$\dot{W}_p$ (kW)	$\dot{W}_n$ (kW)
Tst 151 8-4kW 4-5VDC	58.1	13.4	8.42	0.015	0.134	-0.119
Tst 151 17-9kW 6-5VDC	57.1	15	17.89	0.25	0.272	-0.022
Tst 151 24-2kW 8-5VDC	58.7	15.4	24.3	0.952	0.495	0.456
Tst 152 8-5kW 4-3VDC	63.2	13.8	8.55	0.049	0.124	-0.075
Tst 152 16-9kW 6-5VDC	63	15	17.08	0.153	0.27	-0.117
Tst 152 24-9kW 8-5VDC	63.1	15.4	24.84	0.778	0.5	0.278
Tst 152 26-7kW 8-8VDC	59.6	14.4	26.34	1.268	0.523	0.745
Tst 152 31-4kW 10-0VDC	63.1	16	31.39	1.614	0.714	0.899
Tst 153 16-7kW 6-3VDC	59.2	8.2	16.54	0.28	0.264	0.017
Tst 153 17-3kW 6-5VDC	64.6	10.4	17.4	0.379	0.27	0.11
Tst 153 23-0kW 8-0VDC	58.6	7.6	23.08	0.892	0.442	0.45
Tst 153 26-0kW 8.5-0VDC	64.4	8.6	26.02	1.138	0.505	0.633
Tst 154 8-5kW 4-4VDC	63.4	13.7	8.43	0.061	0.128	-0.067
Tst 154 16-8kW 6-4VDC	63.4	15.1	16.93	0.166	0.258	-0.092
Tst 154 24-8kW 8-5VDC	63.6	15.6	25.01	0.778	0.496	0.282
Tst 154 30-0kW 9-5VDC	63.6	16	30.02	1.353	0.64	0.713

Table 6. *ORC WHR executed test array*

ORC performance

After applying the thermodynamic formulae to the data, ORC efficiency metrics and the efficacy of the zeotropic mixture are evaluated. Table 7 shows these results. Parallel to the expander output, % load, and liquid pump input, the liquid pump efficiency varies from 3% to 10% and expander efficiency varies from 6% to 64%. The off-condition loss in efficiency is large for both liquid pump and expander. The ratio of input to output expander pressure and volume flow rate were also calculated and presented. The higher expander efficiency relates to the expander volume ratio approaching the physical volume ratio of the E22H038B-L-SH. A temperature – entropy plot of the ORC processes with the inlet and outlet temperatures of heat source water and heat sink air overlayed demonstrates the design differential temperature was successful. This is shown in Fig. 6.

The dark blue line, at the top of the diagrams is the water providing heat to evaporate the refrigerant.

The orange line is the ORC working fluid from pump entrance to exit of evaporator (state 1 to 3). The steeply sloped portions are single phase – subcooled to saturated liquid on the left and saturated vapor to superheated vapor on the right. The center section is the phase change from liquid to vapor. The ORC working fluid mixture is zeotropic (evaporating produces a temperature glide). The slopes of the temperature glide and water match confirming the mixture selection and the water flow rate match.

The gray line is the working fluid flowing through the expander (state 3 to 4). If the expander had 100% isentropic efficiency, the slope of this line would be vertical. As seen in the Table 7, maximum expander efficiency occurs at design conditions of T_H ~60°C, T_L ~15°C, and $\dot{Q}$**~30kW**, confirming the selection. However, expander efficiency drops dramatically at off-design conditions. The disconnects between evaporator exit and expander entrance are due to line pressure and temperature loss.

The yellow line is the working fluid flowing through the condenser (state 4 to 1). The steep slope section on the right is removing the superheat of the working fluid leaving the expander. The selected working fluid demonstrated an isentropic or dry characteristic of its saturated vapor T-s curve. At the design condition, the superheat leaving the expander is minimal due to higher expander efficiency and this dry characteristic. The discontinuity between expander exit and condenser inlet are due to pressure and heat loss.

The light blue line is the condenser air temperature as the ORC working fluid is de-superheated, condensed, and subcooled (state 4 to 1). At design condition, the condensing phase change temperature glide is nearly parallel to the air temperature rise.

Test File	η_{th}	η_c	$\%_{Carnot}$ (%)	η_p	η_{ex}	π	$\dot{V}_{ratio}$
151 58.1 (°C)/ 13.4 (°C)/ 8.4kW	-0.01	0.14	-10	0.03	0.06	1.49	1.52
151 57.1 (°C)/ 15.0 (°C)/ 17.9kW	0	0.13	0	0.06	0.28	1.78	1.84
151 58.7 (°C)/ 15.4 (°C)/ 24.3kW	0.02	0.13	14	0.08	0.54	2.1	2.18
152 63.2 (°C)/ 13.8 (°C)/ 8.6kW	-0.01	0.15	-6	0.03	0.19	1.45	1.48
152 63.2 (°C)/ 15.0 (°C)/ 17.1kW	-0.01	0.14	-12	0.06	0.17	1.8	1.86
152 63.1 (°C)/ 15.4 (°C)/ 24.8kW	0.01	0.14	8	0.08	0.44	2.11	2.19
152 59.6 (°C)/ 14.4 (°C)/ 26.3kW	0.03	0.14	21	0.09	0.64	2.18	2.24
152 63.1 (°C)/ 16.0 (°C)/ 31.4kW	0.03	0.14	20	0.1	0.64	2.23	2.32
153 59.2 (°C)/ 8.2 (°C)/ 16.5kW	0	0.15	0	0.06	0.28	2.03	2.09
153 64.6 (°C)/ 10.4 (°C)/ 17.4kW	0.01	0.16	4	0.06	0.38	1.98	2.02
153 58.6 (°C)/ 7.6 (°C)/ 23.1kW	0.02	0.15	13	0.08	0.48	2.41	2.48
153 64.4 (°C)/ 8.6 (°C)/ 26.0kW	0.02	0.17	15	0.08	0.54	2.46	2.53
154 63.4 (°C)/ 13.7 (°C)/ 8.4kW	-0.01	0.15	-5	0.03	0.23	1.48	1.5
154 63.4 (°C)/ 15.1 (°C)/ 16.9kW	-0.01	0.14	-4	0.06	0.19	1.78	1.84
154 63.6 (°C)/ 15.6 (°C)/ 25.0kW	0.01	0.14	8	0.09	0.44	2.11	2.2
154 63.6 (°C)/ 16.0 (°C)/ 30.0kW	0.02	0.14	17	0.1	0.58	2.2	2.3

Table 7. *ORC system, pump, and expander efficiency*

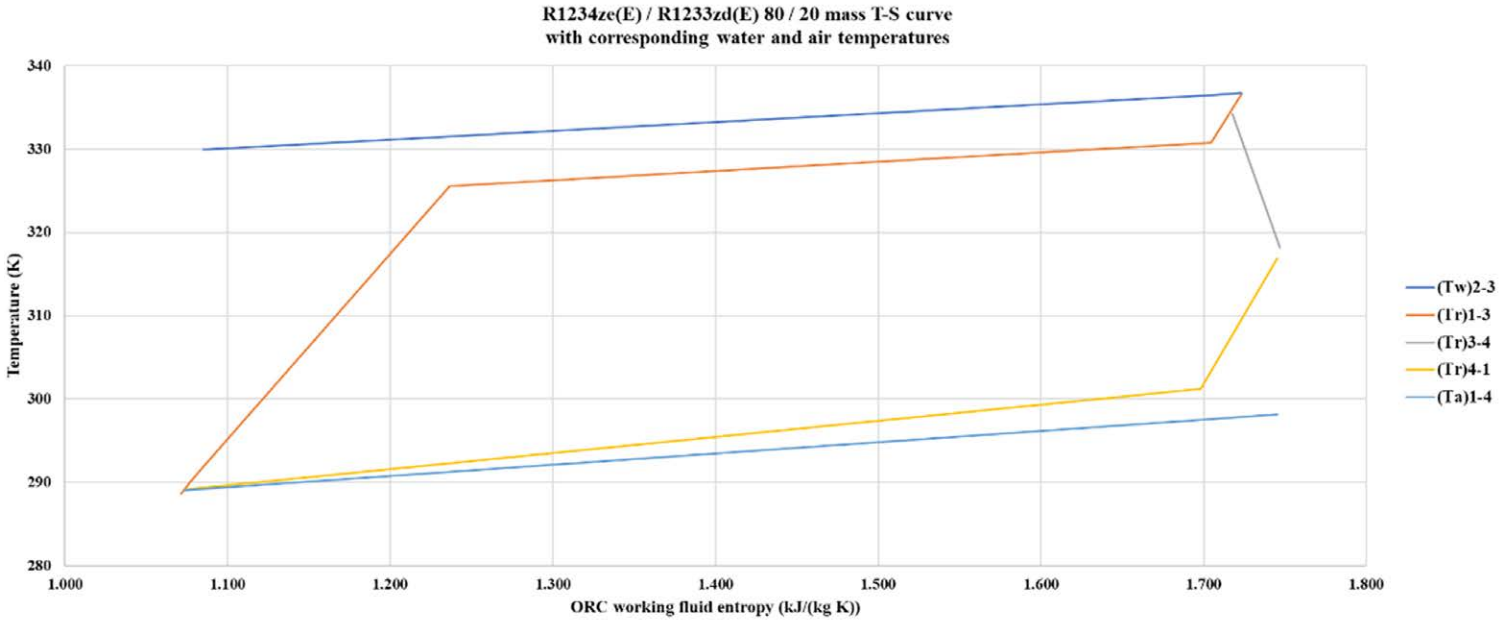

Figure 6. *T-S diagram for Tst 154 30-0kW 9-5VDC*

Exergy destruction analysis

An analysis of exergy destruction rate assists in pointing out the areas of least efficiency. As shown in Table 8, the largest exergy destruction rate is in the evaporator, followed closely by the expander, condenser, and a bit distantly, the pump. The evaporator first has to remove subcooling prior to phase change along the temperature glide. The high liquid specific heat and relatively large average temperature differential during de-subcooling contributes significantly to the evaporator exergy destruction. The low vapor specific heat contributes to lower exergy loss in the condenser. The exergy destruction rate of the expander is directly proportional to product of the mass flow rate and the entropy increase across the expander with the mass flow rate dominating. The liquid pump exergy destruction rates follow the pattern of the expander.

Test	$\dot{I}_p$ (kW)	$\dot{I}_{ev}$ (kW)	$\dot{I}_{ex}$ (kW)	$\dot{I}_c$ (kW)	$\dot{I}_{tot}$ (kW)
151 58.1 (°C)/ 13.4 (°C)/ 8.4kW	0.089	0.604	0.263	0.18	1.136
151 57.1 (°C)/ 15.0 (°C)/ 17.9kW	0.19	0.828	0.624	0.396	2.038
151 58.7 (°C)/ 15.4 (°C)/ 24.3kW	0.368	0.853	0.77	0.654	2.646
152 63.2 (°C)/ 13.8 (°C)/ 8.6kW	0.081	0.69	0.211	0.192	1.173
152 63.2 (°C)/ 15.0 (°C)/ 17.1kW	0.205	1.015	0.688	0.432	2.34
152 63.1 (°C)/ 15.4 (°C)/ 24.8kW	0.372	1.064	0.902	0.707	3.046
152 59.6 (°C)/ 14.4 (°C)/ 26.3kW	0.397	0.935	0.683	0.749	2.765
152 63.1 (°C)/ 16.0 (°C)/ 31.4kW	0.522	1.074	0.824	1.027	3.447
153 59.2 (°C)/ 8.2 (°C)/ 16.5kW	0.206	1.019	0.691	0.426	2.342
153 64.6 (°C)/ 10.4 (°C)/ 17.4kW	0.217	1.183	0.614	0.457	2.471
153 58.6 (°C)/ 7.6 (°C)/ 23.1kW	0.352	1.086	0.907	0.669	3.014
153 64.4 (°C)/ 8.6 (°C)/ 26.0kW	0.39	1.397	0.919	0.812	3.518
154 63.4 (°C)/ 13.7 (°C)/ 8.4kW	0.103	0.675	0.209	0.19	1.178
154 63.4 (°C)/ 15.1 (°C)/ 16.9kW	0.194	1.027	0.648	0.433	2.302
154 63.6 (°C)/ 15.6 (°C)/ 25.0kW	0.37	1.1	0.926	0.74	3.136
154 63.6 (°C)/ 16.0 (°C)/ 30.0kW	0.467	1.101	0.896	0.975	3.439

Table 8. *Exergy destruction rate for components of the ORC system*

WHR system metrics

Transporting heat from the compute equipment to the evaporator requires energy for a water pump. Transporting non-recovered heat from the condenser to atmosphere requires energy for a condenser fan. Pumping a liquid requires relatively small amount of energy while pumping a gas, air, requires relatively large amounts of energy. Table 9 presents the energy performance metrics for the WHR system. Although the ORC produces net positive mechanical work at and above 50% load, the WHR system, when parasitic condenser fan power is included, is an energy consumer even at the best operating conditions. The condenser fan power overwhelms the net power of the ORC system alone. A move to micro-channel condenser coils can reduce the air pressure loss across the condenser and possibly move the design operating conditions to have a net power output.

Test	$\dot{W}_n$ (kW)	$\dot{W}_{cnd\ fan}$ (kW)	$\dot{W}_{wtr\ pmp}$ (kW)	$WHR_{net\ pwr}$ (kW)
151 58.1 (°C)/ 13.4 (°C)/ 8.4kW	-0.119	1.31	0.05	-1.48
151 57.1 (°C)/ 15.0 (°C)/ 17.9kW	-0.022	1.3	0.05	-1.37
151 58.7 (°C)/ 15.4 (°C)/ 24.3kW	0.456	1.29	0.05	-0.88
152 63.2 (°C)/ 13.8 (°C)/ 8.6kW	-0.075	1.29	0.05	-1.42
152 63.2 (°C)/ 15.0 (°C)/ 17.1kW	-0.117	1.27	0.05	-1.44
152 63.1 (°C)/ 15.4 (°C)/ 24.8kW	0.278	1.26	0.05	-1.03
152 59.6 (°C)/ 14.4 (°C)/ 26.3kW	0.745	1.27	0.05	-0.58
152 63.1 (°C)/ 16.0 (°C)/ 31.4kW	0.899	1.25	0.05	-0.4
153 59.2 (°C)/ 8.2 (°C)/ 16.5kW	0.017	1.3	0.05	-1.33
153 64.6 (°C)/ 10.4 (°C)/ 17.4kW	0.11	1.3	0.05	-1.24
153 58.6 (°C)/ 7.6 (°C)/ 23.1kW	0.45	1.3	0.05	-0.9
153 64.4 (°C)/ 8.6 (°C)/ 26.0kW	0.633	1.29	0.05	-0.71
154 63.4 (°C)/ 13.7 (°C)/ 8.4kW	-0.067	1.3	0.05	-1.42
154 63.4 (°C)/ 15.1 (°C)/ 16.9kW	-0.092	1.28	0.05	-1.42
154 63.6 (°C)/ 15.6 (°C)/ 25.0kW	0.282	1.27	0.05	-1.04
154 63.6 (°C)/ 16.0 (°C)/ 30.0kW	0.713	1.26	0.05	-0.6

Table 9. *WHR system metrics*

Verification, validation, and uncertainty quantification

The experimental effort to test the hypothesis of ORC WHR viability requires a process of verification and validation. Test uncertainty analysis is used to objectively validate the measured data quality. An energy balance of the ORC heat and work flows is used to verify the system measurements.

The process of determining test uncertainty follows ASME PTC 19.1-2013 Test Uncertainty. The ORC heat and work flows are calculated values based on formulae defined in the thermodynamic model. Section 7 Uncertainty of a Result and listed formulae are applied [21].

Each of the tests are independent tests with a series of readings over time of a quasi-steady state system. Each result, R, is represented as:

$$R=f(\bar{X}_1, \bar{X}_2, \ldots, \bar{X}_i) \quad (11)$$

where there are i parameters impacting R. Each parameter has an average value with N_i measurements of X_i.

$$\bar{X}_i = 1/N_i \sum_{j=1}^{N_i} X_{(ij)} \quad (12)$$

As the relationship between the result and its parameters cannot be differentiated, sensitivity, θ_i, rate of change of the result with a change of a parameter, is determined numerically

$$\theta_i=\Delta R/(\Delta \bar{X}_i) \quad (13)$$

The expanded uncertainty, $U_{(R,95)}$, at approximately 95% confidence is expressed

$$U_{(R,95)}=2u_R \quad (14)$$

Where

$$u_R=[(b_R)^2+(s_R)^2\ ]^{1/2} \quad (15)$$

The systematic standard uncertainty, b_R, is due to measurement errors that are constant for the duration of testing.

$$b_R=[\sum(i=1)^I(\theta_i\ b_{\overline{X}\ i})^2\ ]^{1/2} \quad (16)$$

These measurement errors are minimized through design of the test and application of the instruments.

The random standard uncertainty, s_R, will approach zero as the number of samples increases. The tests of the ORC system recorded one sample per second for thirty minutes resulting in 1800 samples, >>30 which is defined as a large sample size.

$$s_R=[\sum(i=1)^I(\theta_i\ s_{\overline{X}\ i})^2\ ]^{1/2} \quad (17)$$

Individual random standard uncertainties are related to the sample standard deviation

$$s_{\overline{X}} = s_X/\sqrt{N} \quad (18)$$

Where sample standard deviation, s_X, is

$$s_X\ \sqrt{(\sum(j=1)^N(X_j-\overline{X}\ )^2/(N-1))} \quad (19)$$

The equations for which test uncertainty is estimated include evaporator heat flow, expander work output, condenser heat flow, and the liquid pump work output.

The test uncertainty formulae are applied to each of the tests reported in Table 6. The instrument accuracies reported in Table 5 are used as the perturbation, $\Delta\overline{X}_{\ i}$ to calculate θ_i.

Uncertainty and energy balance results in Table 10 show:

- The expanded test uncertainties of the energy flow calculation, based on measured properties, for both evaporator and condenser are ~1% of calculated energy flow in each test.
- For the expander, the expanded test uncertainties of the energy flow calculation, based on measured properties, are ~10% of calculated energy flow when expander output does not approach zero.
- For the liquid pump, the expanded test uncertainties are ~40% of calculated energy flow. The relatively small differences of temperature across the liquid pump drive this large test uncertainty.
- Theoretically, the sum of energy flows throughout the closed ORC are zero. Test values are <1% of the energy input through the evaporator in each case.
- These results verify and validate the measurement system and measured results.

Test	$\dot{Q}_{ev}$	$U_{R,95}$	$\dot{W}_{ex}$	$U_{R,95}$	$\dot{Q}_c$	$U_{R,95}$	$\dot{W}_p$	$U_{R,95}$	$\sum \dot{E}_{ORC}$
	kW	kW	kW	kW	kW	kW	kW	kW	kW
151 58.1(°C)/ 13.4(°C)/ 8.4kW	8.21	0.09	0.02	0.01	8.29	0.09	0.05	0.02	-0.05
151 57.1(°C)/ 15.0(°C)/ 17.9kW	17.1	0.18	0.25	0.03	17	0.18	0.12	0.05	-0.1
151 58.7(°C)/ 15.4(°C)/ 24.3kW	25.3	0.26	0.95	0.06	24.8	0.26	0.23	0.07	-0.2
152 63.2(°C)/ 13.8(°C)/ 8.6kW	8.11	0.08	0.05	0.01	8.15	0.08	0.05	0.02	-0.04
152 63.2(°C)/ 15.0(°C)/ 17.1kW	16.7	0.17	0.15	0.03	16.8	0.17	0.13	0.04	-0.11
152 63.1(°C)/ 15.4(°C)/ 24.8kW	25.2	0.26	0.78	0.05	24.8	0.25	0.23	0.07	-0.21
152 59.6(°C)/ 14.4(°C)/ 26.3kW	27.3	0.29	1.27	0.06	26.5	0.28	0.25	0.07	-0.22
152 63.1(°C)/ 16.0(°C)/ 31.4kW	33.1	0.34	1.61	0.08	32.1	0.33	0.33	0.09	-0.3
153 59.2(°C)/ 8.2(°C)/ 16.5kW	16	0.16	0.28	0.03	16	0.16	0.12	0.04	-0.11
153 64.6(°C)/ 10.4(°C)/ 17.4kW	16.8	0.17	0.38	0.03	16.7	0.17	0.13	0.04	-12
153 58.6(°C)/ 7.6(°C)/ 23.1kW	23.4	0.24	0.89	0.04	22.8	0.23	0.21	0.06	-0.19
153 64.4(°C)/ 8.6(°C)/ 26.0kW	26.1	0.27	1.14	0.05	25.4	0.26	0.24	0.07	-0.21
154 63.4(°C)/ 13.7(°C)/ 8.4kW	8	0.08	0.06	0.01	8.1	0.08	0.06	0.02	-0.06
154 63.4(°C)/ 15.1(°C)/ 16.9kW	16.5	0.17	0.17	0.03	16.5	0.17	0.12	0.04	-0.11
154 63.6(°C)/ 15.6(°C)/ 25.0kW	25.6	0.26	0.78	0.06	25.2	0.26	0.23	0.07	-0.21
154 63.6(°C)/ 16.0(°C)/ 30.0kW	31.3	0.32	1.35	0.08	30.5	0.31	0.3	0.09	-0.27

Table 10. *ORC test uncertainty, validation, and verification*

Operation with low temperature differential

Test series with T_H=58°C, T_L=27°C were limited to $\dot{Q} \leq 8.8$kW. Above 8.8kW, the liquid head for the pump was lost indicating the condenser practical maximum capacity was reached. With loss of liquid column at pump inlet, ORC working fluid flow stops and the ability to transport waste heat is lost. This is system failure. A revisit to condenser, liquid pump, evaporator, and expander selection assisted in identifying issues. A pressure/enthalpy diagram is useful to visualize the ORC application. Figure 7 shows condenser lines, in yellow, for average and elevated outdoor temperatures and resulting liquid pump lines in blue, evaporator lines in orange, and expander lines in gray.

- The lower heat of condensing for the working fluid at the elevated temperature requires an increase of mass flow rate for a given heat flow. The 11% mass flow rate increase had negligible impact on the condenser performance.
- The required head rise from the pump decreased 38%. The pump is driven by a VFD enabling successful operation at the reduced head and increased flow rate.
- The evaporator inlet subcooling reduced from 35K to 21K while mass flow rate increased 11% for the elevated outdoor temperature. Repeating the evaporator selection at these new conditions showed the evaporator excess capacity increased.
- The expander experienced a reduction in pressure and volume flow rate ratios, from 2.27 to 1.41 and 2.36 to 1.44, respectively, and deserves more detailed investigation.

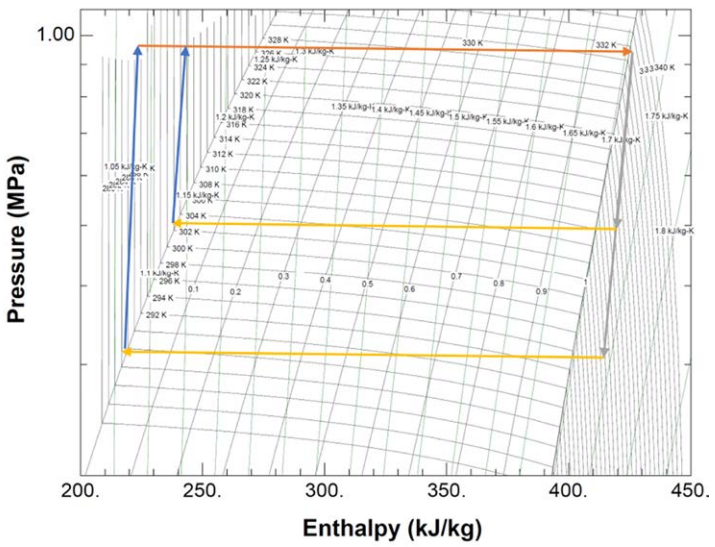

Figure 7. *Pressure vs. Enthalpy plot: R1233zd(E)/R1234ze(E) (20/80)*

Analysis of scroll expander reveals the following relationships. The first is a relative mass flow rate output for a given scroll geometry at varying inlet and outlet pressures. The second provides the critical pressure ratio above which unstable flow conditions exist at the expander inlet port. γ is the specific heat ratio, Cp/Cv. ψ is a flow factor correction. As is the area of the expander inlet port [22].

$$\dot{m}/(\psi A_s)=\sqrt{(2p_h\rho_h)}\ \sqrt{(\gamma/(\gamma-1)\ [(p_l/p_h\ )^{2/\gamma}-(p_l/p_h)^{(\gamma+1)/\gamma}])} \quad (20)$$

$$(p_l/p_h\ )_{crit}=(2/(\gamma+1))^{\gamma/(\gamma-1)} \quad (21)$$

Table 11 illustrates that the Air Squared expander is well matched to operating conditions where ambient temperature, T_L, is between -2°C and 14°C, heat source, TH, is 58°C, and the waste heat load is 30kW. Also, the mass flow rate indicators are relatively constant across the full ambient temperature range. However, the experimentally determined inability to operate at or above 22°C is confirmed by the unstable flow condition as indicated by $(p_l/p_h\ )_{actual} \geq (p_l/p_h)_{crit}$. A quick check was made for pure working fluids R1234ze(E) and R1233zd(E) where both were found to exhibit similar critical pressure ratios.

The critical pressure ratio is a function of specific heat ratio which is given for a working fluid. The implication is that the minimum ΔT for the ORC expander to function avoiding unstable flow condition is ~40K. Thus, the ORC ICT WHR system cannot function if $T_H<T_{amb}$ max+40. For Ashburn, VA, this corresponds to $T_H\geq84$°C. $T_{case}\geq94$°C is implied.

	-2C_Amb 58C water 80-20	14C_Amb 58C water 80-20	22C_Amb 58C water 80-20	30C_Amb 58C water 80-20	Air Squared E22H038B-L-SH	Units
T_{Hwater}K	331.2	331.2	331.2	331.2		(K)
T_{Lamb}C	271.2	287.2	295.2	303.2		(K)
$\dot{V}_3$	0.00323	0.00356	0.00375	0.00395	0.00316	(m^3/s)
$\dot{V}_{ratio}$	4.06	2.36	1.84	1.44	3.25	(-)
π = P_3/P_4	3.91	2.27	1.78	1.41		(-)
Pl/Ph	0.256	0.44	0.563	0.71		(-)
Ph = P3	0.8218	0.8218	0.8218	0.8218		(MPa)
Pl = P4	0.2102	0.3615	0.4627	0.5838		(MPa)
Th = T3	327	327	327	327		(K)
Tl = T4	297.5	307.7	312.9	318.2		(K)
Ƴ = Cp/Cv_3	1.197	1.197	1.197	1.197		(-)
Ƴ = Cp/Cv_4	1.117	1.133	1.145	1.161		(-)
$P4/P3crit_3$	0.565	0.565	0.565	0.565		(-)
$P4/P3crit_4$	0.581	0.578	0.575	0.572		(-)
ρ3	42.79	42.79	42.79	42.79		(kg/m^3)
m_{dot} / $(\psi A_s)_3$	3	3.7	3.8	3.6		($kg/s/m^2$)
displacement					73	cm^3/rev
max speed					2600	rpm

Table 11. *ORC ICT WHR expander relative mass flow rate and critical pressure ratio*

Conclusions

Figure 8 shows the energy flows of the ORC WHR system for test points where T_H 63°C / T_L 15°C excerpted from Tables 6 and 9. Observations:

- Q_{in} is much larger than W_{exp} as predicted by Carnot.
- W_{pmp} is a significant portion of the W_{exp} indicating the pump efficiency requires improvement.
- W_{net} of the ORC is positive above 50% load.
- The parasitic loss of the condenser fan is quite large – moving air to create forced convection is energy intensive.
- The ORC WHR system is a net consumer of power.
- The pair of ~16kW Q_{in} points and pair of ~25kW Q_{in} points were run on separate days demonstrating that, once like setpoints are achieved, the ORC performance replicates.

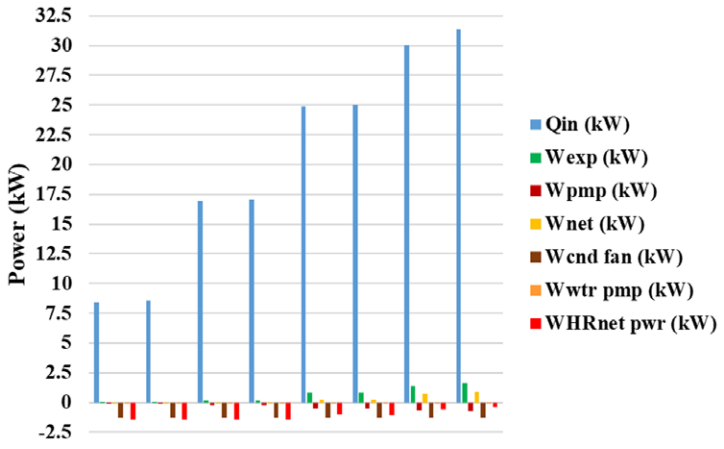

Figure 8. *System Energy Flow for TH 63°C / TL 15°C*

When operating at T_H~58°C, T_L~14°C, and near full load, the ORC can convert ~2% of the waste heat into mechanical energy. Although this may appear negligible, the best data centers consume ~20% of the IT load to transport the waste heat to the outdoors. The ORC provides this cooling with a net output of mechanical energy creating a significant improvement in data center PUE. The regenerative turbine liquid pump consumes ~50% of the energy output of the expander. When the parasitic load to transport the residual waste heat into ambient air is considered, the ORC as a WHR system is an energy consumer.

That being said, in a data center application the WHR system is the cooling system which must operate continuously as load varies from 0% to 100% and ambient temperature varies according to the prevailing weather conditions predicted based on a century of records. The unstable flow limits at the expander inlet in the subject ORC system fall well within the spring, summer, and fall high temperatures expected in Ashburn, VA. Thus, use of ORC WHR as the sole data center cooling means is precluded.

Recommendations

The most critical issue discovered during this ORC WHR testing is the occurrence of unstable flow limits at the expander inlet well within the spring, summer, and fall high temperatures expected of data center locations. Several options can be investigated to resolve this issue:

1. Incorporate an expander bypass so that the system functions as a two-phase pump-assisted thermosyphon when the outdoor temperature falls above that of the inlet flow instability condition limit.
2. Use ORC WHR as supplemental cooling that reduces the energy consumption of the primary data center cooling system when the outdoor temperature falls at or below that of the expander inlet flow instability condition limit.
3. Improve the CPU thermal characteristics to increase T_H avoiding the inlet flow instability condition limit at maximum outdoor temperatures.

Several items can improve the effectiveness of the ORC WHR system.

4. Improve expander off-design efficiency.
5. Improve regenerative turbine pump efficiency at both on-design and off-design conditions.
6. Reduce air flow resistance of the condenser heat exchanger thus reducing the power to drive fan(s).

Acknowledgment

Lorenz Hofmann, PhD, the corresponding author's supervisor, enthusiastically supported and encouraged this research. Dr. Kremer and Dr. Ali of Ohio University provided guidance for the research.

Funding

Vertiv, the corresponding author's employer, provided equipment for the test apparatus, use of instrumentation, and use of test facility.

Nomenclature

1, 2, 3, 4	Subscript, state points, number in series
2s, 4s	Subscript, isentropic state points
A_s	Expander inlet area, m^2
ASHRAE	American Society of Heating, Refrigerating, and Air Conditioning Engineers
b_R	Systematic standard uncertainty of a result
c	Subscript, condenser
C_p	Specific heat at constant pressure, kJ/(kg K)
Cv	Specific heat at constant volume, kJ/(kg K)
CPU	Central processing unit
Δh	Enthalpy change, kJ/kg
η	Efficiency
EH&S	Environmental, Health, and Safety
ev	Subscript, evaporator
ex	Subscript, expander
GWP	Global warming potential
γ	Specific heat ratio
h	Enthalpy, kJ/kg
h	Subscript, high
HVACR	Heating, ventilation, air-conditioning, and refrigeration
İ	Exergy destruction rate, kW
Δk_P	Change of potential energy, kJ/kg
Δk_E	Change of kinetic energy, kJ/kg
l	Subscript, low
ṁ	Mass flow rate, kg/s
ψ	Flow correction factor
N	Number
Ω	Electrical resistance, ohm
ODP	Ozone depletion potential
ORC	Organic Rankine cycle
θ	Sensitivity
p	Subscript, pump
P&ID	Piping and instrumentation diagram
PUE	Power usage effectiveness
PT	Pressure transducer
Q̇	Heat flow, kW
ρ	Density, kg/m^3
R	Result
RTD	Resistance temperature detector
s	Entropy, kJ/(kg K)
S	Standard deviation of the sample
s_R	Random standard uncertainty of a result
T	Temperature, °C, K
TE	Temperature sensor, 100Ω platinum
TC	Temperature sensor, type T thermocouple
T_{case}	Case temperature of CPU
T_H	Temperature of heat source, °C, K
T_L	Temperature of heat sink, °C, K
T_0	Reference temperature, 273.15K
tot	Subscript, total
u_R	Uncertainty of result
$U_{(R,95)}$	Expanded uncertainty at 95% confidence
WHR	Waste heat recovery
Ẇ	Work rate, kW
$\bar{X}$	Average

References

[1] Shehabi, A., et al., United States data center energy usage report LBNL-1005775. Ernest Orlando Lawrence Berkeley National Laboratory: Berkeley, CA, USA, 2016.

[2] Araya, S., et al., Study of a Lab-Scale Organic Rankine Cycle for the Ultra-Low-Temperature Waste Heat Recovery Associated With Data Centers. Journal of Electronic Packaging, 2021. 143(2): p. 021001.

[3] Ebrahimi, K., G.F. Jones, and A.S. Fleischer, A review of data center cooling technology, operating conditions and the corresponding low-grade waste heat recovery opportunities. Renewable and Sustainable Energy Reviews, 2014. 31: p. 622-638.

[4] Lenovo ThinkSystem SD650 Direct Water Cooled Server. Product Guide, 2019.

[5] Banister, J. Why Ashburn Has Emerged as a National Hub for Data Centers. BISNOW, 2017.

[6] ASHRAE, F., Chapter 14 Climatic Design Conditions. 2017: ASHRAE.

[7] ASHRAE, Refrigerants, in ASHRAE Fundamentals Handbook 2017. 2017, ASHRAE: Atlanta, GA.

[8] Rajendran, R. New Refrigerant Alternatives Available Today. E360 Outlook, 2017. 3, 15-16.

[9] Bird, R.B., W.E. Stewart, and E.N. Lightfoot, Macroscopic Balances for Non-isothermal Systems, in Transport Phenomena Revised Second Edition. 2007, John Wiley & Sons, Inc: New York. p. 454-486.

[10] Wang, E., et al., Study of working fluid selection of organic Rankine cycle (ORC) for engine waste heat recovery. Energy, 2011. 36(5): p. 3406-3418.

[11] Chen, H., D.Y. Goswami, and E.K. Stefanakos, A review of thermodynamic cycles and working fluids for the conversion of low-grade heat. Renewable and sustainable energy reviews, 2010. 14(9): p. 3059-3067.

[12] Tchanche, B.F., et al., Fluid selection for a low-temperature solar organic Rankine cycle. Applied Thermal Engineering, 2009. 29(11-12): p. 2468-2476.

[13] McLinden, M.O., et al., A thermodynamic analysis of refrigerants: Possibilities and tradeoffs for Low-GWP refrigerants. International Journal of Refrigeration, 2014. 38: p. 80-92.

[14] Lemmon, E.W., et al. NIST Reference Fluid Thermodynamic and Transport Properties Database (REFPROP): Version 10. 2010.

[15] Air-Squared E22H038B-L-SH. 2018.

[16] ASHRAE, Heat Transfer, in 2017 ASHRAE Handbook Fundamentals. 2017, ASHRAE: Atlanta, GA. p. 4.24-4.25.

[17] Domanski, P.A. and D.A. Yashar, EVAP-COND" NIST (2018). 2018.

[18] Heatcraft, Bohn Coil Performance Charts, in Heatcraft Refrigeration Products LLC. 1988, Heatcraft Refrigeration Products LLC: Stone Mountain, GA.

[19] Ziehl-Abegg, Ziehl-Abegg Axial Fans Main Catalog. 2016, Ziehl-Abegg.

[20] Pumps, M., Bulletin HP31, M. Pumps, Editor. 2016: Plano, IL. p. 2.

[21] ASME, Test Uncertainty. Vol. PTC 19.1-2013. 2013, New York: ASME.

[22] Peng, B., B. Zhu, and V. Lemort, Theoretical and experimental analysis of scroll expander. 2016.

Vertiv.com | **Vertiv Headquarters,** 505 N Cleveland Ave, Westerville, OH 43082, USA

SL-71085 (R06/23)